# A Weighted Adaptive Least-Squares Finite Element Method for the Poisson-Boltzmann Equation

Jehanzeb Hameed Chaudhry[a,1], Stephen D. Bond[b,2], Luke N. Olson[a,3]

[a]*Department of Computer Science, University of Illinois, Urbana, IL 61801*
[b]*Applied Mathematics and Applications Group, Sandia National Laboratories, Albuquerque, NM 87185*



**Abstract**

The finite element methodology has become a standard framework for approximating the solution to the Poisson-Boltzmann equation in many biological applications. In this article, we examine the numerical efficacy of least-squares finite element methods for the linearized form of the equations. In particular, we highlight the utility of a first-order form, noting optimality, control of the flux variables, and flexibility in the formulation, including the choice of elements. We explore the impact of weighting and the choice of elements on conditioning and adaptive refinement. In a series of numerical experiments, we compare the finite element methods when applied to the problem of computing the solvation free energy for realistic molecules of varying size.

*Key words:* Poisson-Boltzmann, finite element, least-squares
*PACS:* 82.20.Wt
*2000 MSC:* 65N30

## 1. Introduction

The Poisson-Boltzmann equation (PBE) is a nonlinear, elliptic partial differential equation (PDE) used to model the electrostatic potential surrounding a fixed biomolecule immersed in an ionic solvent [1, 2]. Calculation of the potential is an important ingredient in many molecular simulations, which necessitates fast, accurate numerical approximation of solutions to the PBE [3–5]. Yet, effective numerical methods for the PBE are challenging to construct due to the complex geometry, discontinuous coefficients, and singularities from point charges that are inherent in the model [6].

A wide variety of numerical schemes have been developed for approximating the solution to the PBE (e.g., see [6] for a survey). Here, we focus on the development and analysis of finite element strategies due to the well developed supporting variational theory. Traditionally the Rayleigh-Ritz or Galerkin finite element method has been the method-of-choice for either the linearized [7, 8] or the non-linear Poisson-Boltzmann equation [9–11]. The Galerkin method is a viable approach, due its relative simplicity, strong theoretical base, and proven results in practice. Even so, there is an opportunity for more advanced approximations when considering other variational formulations of the problem. In this article, we consider a least-squares finite element method [12] for the linearized PBE due to its inexpensive and effective error estimation in adaptive refinement, and because the first-order variables (or fluxes) are specifically expressed in the approximation; this is a useful attribute for many problems.

The first-order system least-squares (FOSLS) finite element method, also known as a least-squares finite element method (LSFEM), is a finite element method wherein the partial differential equation is recast as a first-order system. A quadratic functional based on the residual of the first-order system is then minimized, providing a straightforward error estimator. Finite element methods based on the least-squares approach have been proposed for a variety of PDEs [13], including elliptic problems [14, 15] with discontinuous coefficients [16–18]. Least-squares finite element methods are attractive because they produce symmetric positive definite systems, have no Ladyzhenskaya-Babuŝka-Brezzi (LBB) condition, include a free and sharp error estimator, and allow for direct control of the solution gradient in the approximation.

[1]J. H. Chaudhry, `jhameed2@illinois.edu`, is supported in part by a fellowship from the Computational Science and Engineering program at the University of Illinois, Urbana-Champaign

[2]S. D. Bond, `sdbond@sandia.gov`, is supported in part by the National Science Foundation (CCF 08-30578). Sandia National Laboratories is a multi-program laboratory managed and operated by Sandia Corporation, a wholly owned subsidiary of Lockheed Martin Corporation, for the U.S. Department of Energy's National Nuclear Security Administration under contract DE-AC04-94AL85000.

[3]L. N. Olson, `lukeo@illinois.edu`, is supported in part by the National Science Foundation (DMS 07-46676)

A least-squares finite element method for the PBE was first proposed in [12]. It was shown that the least-squares functional is $H(\text{div}) \times H^1$ equivalent, yet can be used in an existing finite element scheme that uses (more standard) continuous elements in $H^1$. In numerical experiments, an adaptive refinement scheme based on the least-squares functional was shown to yield a faster convergence rate (compared to uniform refinement), especially for solutions with reduced regularity.

In this article we investigate the use of $H(\text{div})$ conforming finite elements and propose a weighted least-squares formulation that leads to optimal convergence of the both the potential and its gradient field. Moreover, we find that the application of our weighted least-squares method results in a balanced convergence of terms in the finite element approximation, leads to modest conditioning in the resulting linear systems, and yields a more accurate calculation of solvation free energy in comparison to other finite element methods.

The remainder of the article is organized as follows. In Section 2, we review the Poisson-Boltzmann equation, including its regularization, linearization, and problem domain, followed by a presentation of a well-posed least-squares formulation of the regularized PBE in Section 3. To support our finite element formulation we also provide an overview of common finite element spaces in Section 4. In Section 5, we compare two least-squares formations: one using piecewise linear elements, and one which uses Raviart–Thomas elements. In Section 6, we review the least-squares formulation of the regularized PBE from the proceeding section, and investigate alternate weightings of the functional. We follow this discussion with an investigation of the relative advantages of this approach in Section 7 and present our conclusions in Section 8.



## 2. Poisson-Boltzmann Equation

We consider the Poisson-Boltzmann equation (PBE) for modeling $n_c$ fixed point charges in a 1:1 electrolyte solvent (e.g. NaCl). The focus here is on the computation of the electrostatic potential $\phi$ governed by the PBE

$$-\nabla \cdot (\epsilon(\mathbf{x})\nabla\phi(\mathbf{x})) + \bar{\kappa}^2(\mathbf{x})\left(\frac{k_B T}{e_c}\right)\sinh\left(\frac{e_c\phi(\mathbf{x})}{k_B T}\right) = 4\pi\sum_{i=1}^{n_c} Q_i\delta(\mathbf{x}-\mathbf{x}_i),$$
$$\lim_{\|\mathbf{x}\|\to\infty}\phi(\mathbf{x}) = 0. \tag{1a}$$

The Boltzmann constant is denoted by $k_B$, temperature by $T$, and the charge of a proton by $e_c$. The value of the $i^{\text{th}}$ charge, $Q_i$, centered at position $x_i$, depends on the particular molecule being modeled. We consider a modeling domain that is subdivided into a molecular region, $\Omega_m$, a solvent region, $\Omega_s$, and an interface between the two, denoted by $\Gamma$. This decomposition is depicted in Figure 1. Using this splitting, we define the dielectric coefficient, $\epsilon(\mathbf{x})$, and modified Debye-Hückel parameter, $\bar{\kappa}(\mathbf{x})$, over $\Omega_m \cup \Omega_s$ by the piecewise constant functions

$$\epsilon(\mathbf{x}) = \begin{cases}\epsilon_m, & \mathbf{x}\in\Omega_m,\\ \epsilon_s, & \mathbf{x}\in\Omega_s,\end{cases} \quad \text{and} \quad \bar{\kappa}^2(\mathbf{x}) = \begin{cases}0, & \mathbf{x}\in\Omega_m,\\ \bar{\kappa}_s^2, & \mathbf{x}\in\Omega_s.\end{cases}$$

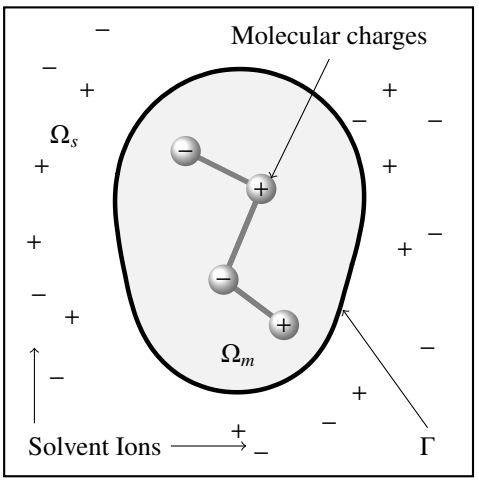


Figure 1: Problem domain

For practical computations, the unbounded solvent domain, $\Omega_s$, is typically truncated at a finite radius from the center of mass of the molecule and the equation is solved by imposing Dirichlet boundary conditions. Using a change of variables, $\tilde{u}(\mathbf{x}) = e_c\phi(\mathbf{x})/k_BT$, this results in a dimensionless Poisson-Boltzmann equation on the truncated domain, $\Omega = \Omega_m \cup \Omega_s \cup \Gamma$:

$$-\nabla \cdot (\epsilon(\mathbf{x})\nabla\tilde{u}(\mathbf{x})) + \bar{\kappa}^2(\mathbf{x}) \sinh \tilde{u}(\mathbf{x}) = \frac{4\pi e_c}{k_BT} \sum_{i=1}^{n_c} Q_i \delta(\mathbf{x} - \mathbf{x}_i), \quad \mathbf{x} \in \Omega_m \cup \Omega_s, \tag{2a}$$

$$\tilde{u}(\mathbf{x}) = g(\mathbf{x}), \qquad \mathbf{x} \in \partial\Omega. \tag{2b}$$

Here, the boundary conditions are given by

$$g(\mathbf{x}) = \frac{e_c}{k_BT} \sum_{i=1}^{n_c} \frac{Q_i}{\epsilon_s|\mathbf{x} - \mathbf{x}_i|} \exp\left(\frac{-\bar{\kappa}_s|\mathbf{x} - \mathbf{x}_i|}{\sqrt{\epsilon_s}}\right), \tag{3}$$

which matches the asymptotic behavior of the non-truncated problem [19].

The $\delta$-functions in equation (2) are computationally challenging and are addressed by regularization [19]. Consider the decomposition of $\tilde{u}$ into

$$\tilde{u} = u + u_c, \tag{4}$$

where $u$ is an unknown smooth function and $u_c$ is a known singular function (the Coulomb potential). Here, $u_c$ contains the singularities in $\tilde{u}$ and is the analytic solution to the more tractable Poisson equation

$$-\epsilon_m \nabla \cdot \nabla u_c(\mathbf{x}) = \frac{4\pi e_c}{k_BT} \sum_{i=1}^{n_c} Q_i \delta(\mathbf{x} - \mathbf{x}_i). \tag{5}$$

By combining (4) with (2), and linearizing the hyperbolic sine term, we obtain the linear regularized Poisson-Boltzmann equation

$$-\nabla \cdot \epsilon(\mathbf{x})\nabla u(\mathbf{x}) + \bar{\kappa}^2(\mathbf{x})u(\mathbf{x}) = \nabla \cdot (\epsilon(\mathbf{x}) - \epsilon_m)\nabla u_c(\mathbf{x}) - \bar{\kappa}^2(\mathbf{x})u_c(\mathbf{x}), \quad \mathbf{x} \in \Omega_s \cup \Omega_m, \tag{6a}$$

$$u(\mathbf{x}) = g(\mathbf{x}) - u_c(\mathbf{x}), \qquad \mathbf{x} \in \partial\Omega, \tag{6b}$$

$$\left[\!\left[ \epsilon(\mathbf{x}) \frac{\partial u(\mathbf{x})}{\partial \mathbf{n}} \right]\!\right]_\Gamma = -\left[\!\left[ \epsilon(\mathbf{x}) \frac{\partial u_c(\mathbf{x})}{\partial \mathbf{n}} \right]\!\right]_\Gamma, \qquad \mathbf{x} \in \Gamma. \tag{6c}$$

For a point on the interface, $\mathbf{x} \in \Gamma$, the jump is defined as

$$[\![ v(\mathbf{x}) ]\!]_\Gamma = \lim_{\theta \to 0^+} v(\mathbf{x} + \theta\mathbf{n}) - v(\mathbf{x} - \theta\mathbf{n}),$$

where $\mathbf{n}$ is the surface normal. Consequently, we see that the non-zero jump in the flux is particularly challenging computationally. One focus of this article is to highlight the representation of the flux in a finite element approximation.

## 3. Least-squares finite element formulation

A least-squares finite element method (LSFEM) is an alternative to Galerkin and mixed Galerkin finite element methods [13]. In the first-order system approach, LSFEMs transform a (typically second-order) PDE into a first-order system and a functional is then formed based on the $L^2$-norm of the residual equations. One outcome of this approach is that the resulting bilinear form is often equivalent to practical Sobolev inner products such as $H^1$ or $H(\mathrm{div})$. As a result, the discrete inf-sup condition of Ladyzhenskaya-Babuŝka-Brezzi [20] is automatically satisfied due to the resulting coercivity and continuity of the bilinear form, unlike mixed methods. Thus, basic finite element spaces, such as continuous piecewise linear polynomials, may be used for all variables; this is a notable advantage of the LSFEM.

The ellipticity of the functional guarantees the *best* solution in the associated finite element space. This optimality of the solution allows us the choice of a large number of finite element spaces. For example if the method is $H(\mathrm{div}) \times H^1$ elliptic (defined in (8)), then $H(\mathrm{div})$ conforming Raviart–Thomas elements are the natural choice, yet basic piecewise linear polynomials may also be competitive. We address this for the PBE in Section 5.

There are a number of other practical advantages of using LSFEMs. The linear system obtained from a LSFEM discretization is symmetric and positive-definite, making it well suited for iterative Krylov methods. Moreover, the least-squares functional also provides a local and inexpensive *a posteriori* error estimate which may be used to guide adaptive refinement. Conversely, the transformation to a first-order systems introduces new variables, invariably increasing the computational

complexity of obtaining the solution. Often this is not a significant disadvantage since the new variables are often of interest in many applications and since the variables enable equivalence in a useful norm.

A LSFEM for the PBE is described in detail in [12]. Here, we summarize the formulation. For a well-posed least-squares formulation to system (6), we define a first-order variable $\mathbf{q}$, with a normal component that is both continuous across the interface and also satisfies the interface condition required by the RPBE. To ensure these conditions, we define $\mathbf{q} = \epsilon(\mathbf{x})\nabla u + (\epsilon(\mathbf{x}) - \epsilon_m)\nabla u_c$, which results in

$$\mathbf{q}/\epsilon(\mathbf{x}) - \nabla u = ((\epsilon(\mathbf{x}) - \epsilon_m)/\epsilon(\mathbf{x}))\nabla u_c, \qquad \text{in } \Omega, \tag{7a}$$

$$-\nabla \cdot \mathbf{q} + \bar{\kappa}^2(\mathbf{x})u = -\bar{\kappa}^2(\mathbf{x})u_c, \qquad \text{in } \Omega, \tag{7b}$$

$$u = g - u_c, \qquad \text{on } \partial\Omega, \tag{7c}$$

$$\mathbf{n} \times \mathbf{q} = \mathbf{n} \times (\epsilon_s \nabla g + (\epsilon(\mathbf{x}) - \epsilon_m)\nabla u_c), \qquad \text{on } \partial\Omega. \tag{7d}$$

Now equations (6c) and (7) imply

$$[\![\mathbf{q} \cdot \mathbf{n}]\!]_\Gamma = 0, \quad \mathbf{x} \in \Gamma.$$

We denote the standard Sobolev spaces as $L^2(\Omega)$ and $H^k(\Omega)$, for $k \geq 0$. $H^k(\Omega)$ consists of functions over $\Omega$ whose (weak) derivatives are in $L^2(\Omega)$. The norms on $L^2(\Omega)$ and $H^k(\Omega)$ are expressed as $\|\cdot\|_{0,\Omega}$ and $\|\cdot\|_{k,\Omega}$, with the $L^2(\Omega)$ inner product written $(\cdot,\cdot)_{0,\Omega}$. In addition, we define the Hilbert spaces

$$H(\mathrm{div};\Omega) := \{\mathbf{q} \in L^2(\Omega)^3 : \nabla \cdot \mathbf{q} \in L^2(\Omega)\}, \tag{8}$$

$$H(\mathrm{curl};\Omega) := \{\mathbf{q} \in L^2(\Omega)^3 : \nabla \times \mathbf{q} \in L^2(\Omega)^3\}, \tag{9}$$

$$H_0(\mathrm{div};\Omega) := \{\mathbf{q} \in H(\mathrm{div};\Omega) : \mathbf{n} \cdot \mathbf{q} = 0 \text{ on } \partial\Omega\}, \tag{10}$$

$$H_0^1(\Omega) := \{u \in H^1(\Omega) : u = 0 \text{ on } \partial\Omega\}, \tag{11}$$

with norms

$$\|\mathbf{q}\|^2_{\mathrm{curl},\Omega} = \|\mathbf{q}\|^2_{0,\Omega} + \|\nabla \times \mathbf{q}\|^2_{0,\Omega}, \tag{12}$$

$$\|\mathbf{q}\|^2_{\mathrm{div},\Omega} = \|\mathbf{q}\|^2_{0,\Omega} + \|\nabla \cdot \mathbf{q}\|^2_{0,\Omega}, \tag{13}$$

$$\|u\|^2_{1,\Omega} = \|u\|^2_{0,\Omega} + \|\nabla u\|^2_{0,\Omega}. \tag{14}$$

The least-squares functional based on (7) is as follows. For $\mathbf{q} \in H_0(\mathrm{div};\Omega)$ and $u \in H_0^1(\Omega)$, we define

$$G(\mathbf{q}, u; u_c) = \left\| \frac{\mathbf{q}}{\epsilon} - \nabla u - \frac{\epsilon - \epsilon_m}{\epsilon}\nabla u_c \right\|^2_{0,\Omega} + \left\| -\nabla \cdot \mathbf{q} + (u + u_c)\bar{\kappa}^2 \right\|^2_{0,\Omega}. \tag{15}$$

The solution of (7) solves the minimization problem

$$G(\mathbf{q}, u; u_c) = \min_{(\mathbf{r},v) \in H_0(\mathrm{div};\Omega) \times H_0^1(\Omega)} G(\mathbf{r}, v; u_c) \tag{16}$$

and leads to the variational problem

$$\mathcal{F}(\mathbf{q}, u; \mathbf{r}, v) = \ell(\mathbf{r}, v), \tag{17}$$

where the bilinear form $\mathcal{F}$ and linear functional $\ell$ are

$$\mathcal{F}(\mathbf{q}, u; \mathbf{r}, v) = (\mathbf{q}/\epsilon - \nabla u, \mathbf{r}/\epsilon - \nabla v)_{0,\Omega} + (-\nabla \cdot \mathbf{q} + \bar{\kappa}^2 u, -\nabla \cdot \mathbf{r} + \bar{\kappa}^2 v)_{0,\Omega}, \tag{18}$$

$$\ell(\mathbf{r}, v) = (-\bar{\kappa}^2 u_c, -\nabla \cdot \mathbf{r} + \bar{\kappa}^2 v)_{0,\Omega} + (((\epsilon - \epsilon_m)/\epsilon)\nabla u_c, \mathbf{r}/\epsilon - \nabla v)_{0,\Omega}. \tag{19}$$

As a result, the variational problem (17) is well-posed since $G(\mathbf{q}, u; 0)^{\frac{1}{2}}$ defines a norm equivalent to the $H(\mathrm{div}) \times H^1$-norm [12].

## 4. Description of FEM Spaces

Since the least-squares functional is $H(\mathrm{div}) \times H^1$ equivalent, Cea's Lemma ensures the best approximation in any finite-dimensional subspace of $H(\mathrm{div}) \times H^1$. Here we consider spaces of piecewise polynomials on a tetrahedral mesh and denote the spaces corresponding to the discrete solutions $\mathbf{q}_h$ and $u_h$ as $m$-dimensional $\mathbf{W}^h$ and $n$-dimensional $V^h$ respectively, with


Figure 2: Vector spaces and finite elements



$\mathbf{W}^h \subset H(\text{div})$ and $V^h \subset H^1$. Further, we denote basis functions of $\mathbf{W}^h$ by $\boldsymbol{\psi}(\mathbf{x})$ and those of $V^h$ by $\phi(\mathbf{x})$. Then any function in these subspaces is represented as

$$\mathbf{q}_h = \sum_{i=1}^{m} q_i \boldsymbol{\psi}_i, \quad u_h = \sum_{i=1}^{n} u_i \phi_i. \tag{20}$$

A common choice for $H^1$ subspaces are globally continuous piecewise linear functions — i.e. the restriction of such functions on any tetrahedron $T$ belongs to $\mathbb{P}_1(T)$, where $\mathbb{P}_1(T)$ is the space of degree one polynomials. The relationship between spaces $H(\text{div})$, $H(\text{curl})$, and $(H^1)^3$ is illustrated in Figure 2a. A common choice of basis that is widely available in many software packages is to represent each vector component as a continuous piecewise linear function (a 12-dimensional vector field over the tetrahedron). However, while continuous $\mathbb{P}_1^3$ elements are straightforward, another popular alternative are the vector-valued Raviart–Thomas elements [21, 22]. A vector-valued function belongs to $H(\text{div})$ only if its normal component is continuous across any surface in $\Omega$ and Raviart–Thomas elements are designed to satisfy this requirement by imposing normal continuity. That is,

$$\begin{aligned} RT_k := \{&\zeta \in L^2(\Omega)^3;\ \zeta|_T = c + kx, c \in \mathbb{P}_k^3, k \in \mathbb{P}_k, x \in T, \\ &\zeta \cdot n \text{ is continuous across neighboring faces}\}. \end{aligned} \tag{21}$$

The set of lowest order Raviart–Thomas elements, $RT_0$, is a four dimensional subspace of $\mathbb{P}_1^3(T)$ where each element is of the form $\mathbf{p} = \mathbf{c} + k\mathbf{x}$ with $\mathbf{c} \in \mathbb{R}^3, k \in \mathbb{R}$. The normal component $\mathbf{p} \cdot \mathbf{n}$ is constant on each tetrahedron face and identifies each degree-of-freedom. That is, zeroth order moments of $\mathbf{p} \cdot \mathbf{n}$, $\int_{\text{face}} \mathbf{p} \cdot \mathbf{n}\, d\gamma$, define the degrees-of-freedom. Raviart–Thomas elements are not tangentially continuous across the element boundary, and hence contain discontinuous functions; they impose only the continuity required by $H(\text{div})$. Figure 2b illustrates the degrees-of-freedom on a tetrahedron for both $\mathbb{P}_1$ and $RT_0$ spaces.

## 5. On the use of Piecewise Linear and Raviart–Thomas Elements

In this section we consider the merits of $\mathbb{P}_1$ and $RT_0$ elements for representing the flux $\mathbf{q}$. We consider a tetrahedral mesh of $\Omega$ generated using the Geometry-preserving Adaptive Mesher (GAMer), which is designed to produce simplicial meshes of molecular volumes and interfaces [23].

The least-squares functional exhibits good convergence properties, as shown in [12], when using $\mathbb{P}_1$ elements [12]. However the problem was shown to be $H(\text{div}) \times H^1$ equivalent, and $\mathbb{P}_1$ elements cannot converge to the continuum solution if the flux $\mathbf{q}$ is in $H(\text{div})\backslash(H^1(\Omega))^3$, as shown in [24]. Hence, for robustness of the numerical method, we advocate the use of $H(\text{div})$ conforming elements for solving the PBE.

Next we examine some experimental results for the $\mathbb{P}_1$ and $RT_0$ elements. In each experiment, we solve for the regularized potential $u$ and flux $\mathbf{q}$, while strongly imposing the Dirichlet boundary conditions onto the finite element space. The first test case is that of a Born ion, for which one can derive an analytical solution to the linearized form of the PBE [25, 26]. In this case, the computational domain consists of a spherical solute of radius $R$ with a single point charge $Q_1$ at its center, and the solute is surrounded by a large spherical solvent domain, $\Omega_s$, as depicted in Figure 3a.

For a more realistic and non-symmetric geometry, we examine in a second test case of a methanol molecule [27]. The methanol domain is constructed from a model with three groups of atoms of differing radii: two with positive charges, and one with a negative charge, for a total net charge of zero.

Finally, to compare the methods on more realistic and complex geometries, we perform a sequence of experiments with four molecules obtained from the Protein Data Bank [28]: 1bor, 1vii, 1sh1 and 1cbn. Figure 3b shows the structure of the

1sh1 molecule, surrounded by a slice of the molecular surface (the complete surface is shown in Figure 4a). Figure 4b is an enlarged view of the irregular and complicated mesh inside the molecular region (gray), and a small part of the surrounding solvent region (white). The other three remaining molecules have similarly complex geometries.

For the Born ion and methanol, we set parameters $\epsilon_m = 1$, $\epsilon_s = 78$, and $\bar{\kappa}_s = 0.918168$, which corresponds to an ionic strength of 0.1 M. These values are consistent with those used in [12]. For the other four molecules, we set $\epsilon_s = 80$.

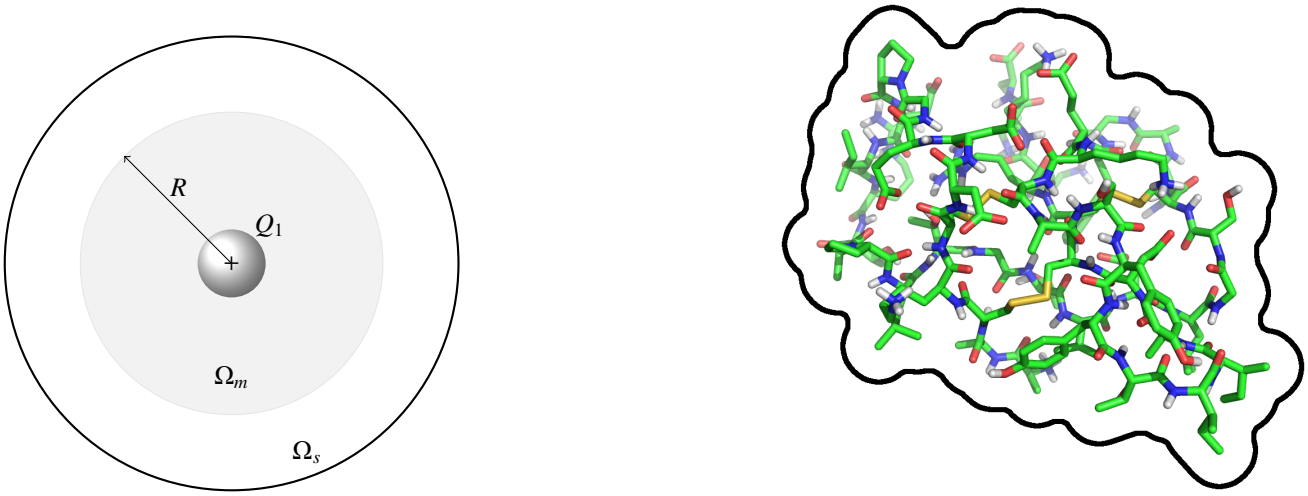


(a) Born Ion (b) 1sh1

Figure 3: Schematic of problem domains

*Convergence in the $L^2$-norm and least-squares norm*

The convergence rates presented in Table 1 highlight the optimality of the LSFEM for the problem. The method achieves $O(h^2)$ convergence in the scalar potential $u$ in the $L^2$-norm for both $\mathbb{P}_1$ and $RT_0$.

| | $L^2$-norm | | | | LS-norm | | | |
|---|---|---|---|---|---|---|---|---|
| | $\mathbb{P}_1$ | | $RT_0$ | | $\mathbb{P}_1$ | | $RT_0$ | |
| $h/h_0$ | Value | Rate | Value | Rate | Value | Rate | Value | Rate |
| 1 | 284.4 | | 303.5 | | 383.3 | | 378.6 | |
| 1/2 | 81.6 | 1.80 | 84.0 | 1.85 | 189.5 | 1.02 | 189.0 | 1.00 |
| 1/4 | 21.5 | 1.92 | 21.8 | 1.94 | 94.4 | 1.01 | 94.3 | 1.00 |
| 1/8 | 5.4 | 1.99 | 5.5 | 1.99 | 46.9 | 1.01 | 46.9 | 1.01 |

Table 1: Convergence in $L^2$ and least-squares norms for the Born Ion

Since the least-squares functional is an error estimator, we also observe convergence by monitoring the least-squares norm. Specifically, the least-squares functional measures the error in the norm $\|(\mathbf{q}^h, u^h)\|_{\mathrm{LS}} = G(\mathbf{q}^h - \mathbf{q}, u^h - u; 0)^{\frac{1}{2}}$.

Since we are using linear polynomials and the lowest-order $RT_0$ elements, the optimal convergence in an $H(\mathrm{div}) \times H^1$ equivalent norm is expected to be $O(h)$. The convergence for the Born ion and methanol is summarized in Tables 1 and 2, which shows near optimal performance in both cases. In the tables, $h_0$ represents the mesh size parameter for the coarsest mesh. We observe that using $RT_0$ elements yields a slightly more accurate solution for methanol.

For the other four molecules, the initial mesh generated by GAMer is fine enough that uniform octasection refinement is only feasible for a couple of mesh refinements. For this reason, we use uniform (longest edge) bisection refinement for these molecules. In computing convergence rates, we use the average value of the radius of the elemental circumspheres, $h$. Table 3 shows the convergence rate for these four molecules. Refinement level indicates how many times the mesh has been refined, where level 0 is the initial mesh. Once again we find that $RT_0$ elements are more accurate, and converge at a higher rate.

The slightly higher accuracy of $RT_0$ elements is not surprising since we are looking for a solution in $H(\mathrm{div})$ and $RT_0$ elements approximate $H(\mathrm{div})$ better than $\mathbb{P}_1$ by allowing inter-element jumps in the flux function $\mathbf{q}$. $RT_0$ elements offer a

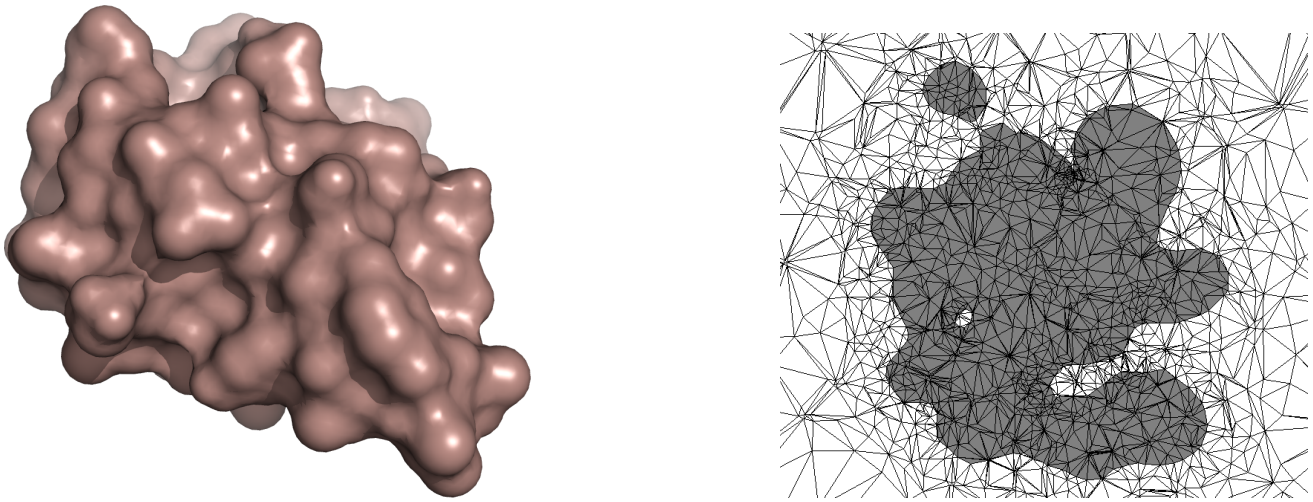

(a) (b)

Figure 4: Geometry of the 1sh1 molecule

| | $\mathbb{P}_1$ | | $RT_0$ | |
|---|---|---|---|---|
| $h/h_0$ | Value | Rate | Value | Rate |
| 1 | 228.0 | | 211.7 | |
| 1/2 | 142.8 | 0.68 | 121.1 | 0.81 |
| 1/4 | 82.2 | 0.80 | 63.9 | 0.92 |
| 1/8 | 45.4 | 0.86 | 32.6 | 0.97 |

Table 2: Convergence in the least-squares norm for methanol

more flexible space for minimization of the least-squares functional with fewer restrictions on continuity. We note that the convergence rate for 1sh1 and 1cbn is below the optimal $O(h)$. This is possibly due to the decreased regularity of the solution, as the coefficients $\epsilon$ and $\bar{\kappa}$ are discontinuous at the interface, $\Gamma$. Moreover, the presence of corner singularities at the interface may also be playing a role in the decreased convergence rate, c.f. Remark 2.

*Cost of solving the discrete problems*

We also need to take into account the computational cost of solving the resulting discrete problems. For many iterative solvers, this cost can be estimated using two properties: the number of non-zeros in the matrix, and its condition number. The number of non-zeros which is an indicator of the efficiency of a matrix-vector multiply, is nearly identical for both elements as shown in Table 4. For all six test cases, the ratio of non-zeros for $RT_0$ and $\mathbb{P}_1$ was nearly constant with a value of approximately 0.9.

One attractive quality of a least-squares finite element approximation is that the resulting matrix problems are symmetric and positive definite. However the choice of elements affects the conditioning of the linear systems. In Table 5, we report the condition number for the coarsest mesh for $\mathbb{P}_1$ and $RT_0$ approximations; the condition number for a system arising from a LSFEM is known to be $O(h^{-2})$ [14]. The $\mathbb{P}_1$ approximation yields systems with improved conditioning compared to $RT_0$, as mentioned in [24]. However, there exist preconditioners that are designed specifically for face elements [29, 30], hence this is not a significant factor in deciding which elements to use, as argued in [24]. For the remainder of the article, we use $RT_0$ elements for the LSFEM, unless otherwise specified.

## 6. Comparison of different weightings of the LSFEM Functional

In this section we investigate how different weights on the two terms of the least-squares functional affects the properties of the finite element solution. To motivate this section, we write equation (7) in a new form,

$$\alpha(\mathbf{x})(\mathbf{q} - \epsilon(\mathbf{x})\nabla u) = \alpha(\mathbf{x})((\epsilon(\mathbf{x}) - \epsilon_m))\nabla u_c, \quad \text{in } \Omega, \tag{22a}$$

$$-\nabla \cdot \mathbf{q} + \bar{\kappa}^2(\mathbf{x})u = -\bar{\kappa}^2(\mathbf{x})u_c, \quad \text{in } \Omega. \tag{22b}$$

| Refinement level | 1bor | | 1vii | | 1sh1 | | 1cbn | |
|---|---|---|---|---|---|---|---|---|
| | $\mathbb{P}_1$ | $RT_0$ | $\mathbb{P}_1$ | $RT_0$ | $\mathbb{P}_1$ | $RT_0$ | $\mathbb{P}_1$ | $RT_0$ |
| 1 | 0.96 | 1.92 | 0.82 | 0.86 | 0.97 | 0.97 | 0.84 | 0.77 |
| 2 | 0.75 | 1.24 | 1.10 | 1.20 | 0.66 | 0.77 | 0.60 | 0.74 |
| 3 | 0.78 | 0.95 | 1.17 | 1.17 | 0.75 | 0.77 | 0.69 | 0.71 |

Table 3: Convergence rates in the least-squares norm for 1bor, 1vii, 1sh1 and 1cbn

| | Born Ion | | | Methanol | | |
|---|---|---|---|---|---|---|
| $h/h_0$ | $\mathbb{P}_1$ | $RT_0$ | ratio | $\mathbb{P}_1$ | $RT_0$ | ratio |
| 1 | 4.775E+05 | 4.270E+05 | 0.89 | 4.763E+05 | 4.264E+05 | 0.90 |
| 1/2 | 3.774E+06 | 3.406E+06 | 0.90 | 3.768E+06 | 3.401E+06 | 0.90 |
| 1/4 | 2.999E+07 | 2.721E+07 | 0.91 | 2.995E+07 | 2.717E+07 | 0.91 |
| 1/8 | 2.390E+08 | 2.174E+08 | 0.91 | 2.387E+08 | 2.171E+08 | 0.91 |

Table 4: Number of non-zeros for $RT_0$ versus $\mathbb{P}_1$

This leads to the LSFEM functional,

$$G_\alpha(\mathbf{q}, u; u_c) = \|\alpha\mathbf{q} - \alpha\epsilon\nabla u - \alpha((\epsilon - \epsilon_m))\nabla u_c\|^2_{0,\Omega} + \| - \nabla\cdot\mathbf{q} + \bar{\kappa}^2 u + \bar{\kappa}^2 u_c\|^2_{0,\Omega}. \tag{23}$$

Here the first equation in (22), or alternatively the first term of the LSFEM functional (23), is weighted by a factor $\alpha(\mathbf{x})$. If $\alpha(\mathbf{x}) = 1/\epsilon(\mathbf{x})$, we recover equation (7).

The primary motivation for choosing $\alpha(\mathbf{x}) = 1/\epsilon(\mathbf{x})$ in [12] is the observation that $\epsilon(\mathbf{x}) \geq 1$, which implies that $\alpha(\mathbf{x}) \leq 1$, and so the term in the LSFEM functional corresponding to equation (22a) is given a decreased weight. This has the effect of overweighting the minimization of (22b), and hence we expect a more accurate potential $u$. However, we also expect this to lead to a less accurate resolution of the flux $\mathbf{q}$. An alternative weighting that we investigate here is to use $\alpha(\mathbf{x}) = 1/\sqrt{\epsilon}$. This redistributes the weight to the flux term (22a), leading to a more accurate approximation to $\mathbf{q}$, while maintaining similar convergence rates in each variable. We confirm these observation for the Born ion using uniform refinement, as reported in Table 6, where we also show the weighting $\alpha = 1$ for comparison.

**Remark 1.** *The discontinuity in coefficient functions $\bar{\kappa}$ and $\epsilon$ results in solutions that are less smooth. While the LSFEM* (7) *results in the best approximation in a given finite-element space, convergence of the method cannot be guaranteed using piecewise linear elements. One possible way to overcome the interface challenge is to explicitly represent the jump conditions in (6c) [31]. Since the solution belongs to $H^2$ when restricted to $\Omega_m$ or $\Omega_s$, the dual domain approach to the LSFEM defines functionals on each of the two domains, while interface terms are added to couple the problems. Letting $(\mathbf{q}_m, u_m)$ and $(\mathbf{q}_s, u_s)$ be the restriction of the solution in $\Omega_m$ and $\Omega_s$, respectively, we define the least-squares functional $\hat{G}$ as*

$$\begin{aligned}\hat{G}(\mathbf{q}, u; u_c) = &\sum_{i=m,s} (\|\mathbf{q}_i/(\epsilon) - \epsilon\nabla u_i/\epsilon - ((\epsilon - \epsilon_m)/\epsilon)\nabla u_c\|^2_{0,\Omega_i} + \| - \nabla\cdot\mathbf{q}_i + \kappa^2 u_i + \kappa^2 u_c\|^2_{0,\Omega_i}) \\ &+ \frac{1}{h^{1+c_0}}\int_\Gamma [\![u]\!]^2_\Gamma \, d\Gamma + \frac{1}{h^{c_1}}\int_\Gamma [\![\mathbf{q}.n]\!]^2_\Gamma \, d\Gamma,\end{aligned} \tag{24}$$

*with $c_0, c_1 > 0$. This method requires a more complex implementation as compared to the single domain formulation, due to the presence of the interface term, and the use of two degrees-of-freedom at each vertex at the interface $\Gamma$, as shown in Figure 5.*

Next we examine the conditioning of the linear systems due to the different weightings. As we have noted earlier, the conditioning of the linear system greatly affects the performance of the linear solver. As before, we examine the condition number at the coarsest mesh level, for the Born ion and for methanol. The condition numbers are approximated by estimating the ratio of the largest and smallest eigenvalues of the linear system using the Lanczos method. The results, shown in Table 7, show that the weight $\alpha = 1/\sqrt{\epsilon}$ leads to better conditioned systems.

Finally we examine the conditioning as the ratio $\epsilon_s/\epsilon_m$ is varied for the Born ion for the two weightings. Motivated by the theory outlined in [12], which shows that the coercivity and continuity bounds for the least-squares finite element method are dependent on the values of $\epsilon_s$ and $\epsilon_m$, we set $\epsilon_m = 1$, and vary $\epsilon_s$ over a range of physically realistic values. We see that the

| | Born Ion | Methanol | 1bor | 1vii | 1sh1 | 1cbn |
|---|---|---|---|---|---|---|
| $\mathbb{P}_1$ | 1.07E+06 | 1.26E+06 | 1.29E+08 | 1.30E+08 | 1.06E+08 | 8.79E+07 |
| $RT_0$ | 8.07E+09 | 8.66E+09 | 5.05E+13 | 2.15E+15 | 5.22E+13 | 3.18E+13 |

Table 5: Conditioning of Linear Systems

| | $L_2$ error in $u^h$ | | | $L_2$ error in $\mathbf{q}^h$ | | |
|---|---|---|---|---|---|---|
| $h/h_0$ | $\alpha = 1/\epsilon$ | $\alpha = 1/\sqrt{\epsilon}$ | $\alpha = 1$ | $\alpha = 1/\epsilon$ | $\alpha = 1/\sqrt{\epsilon}$ | $\alpha = 1$ |
| 1 | 303.5 | 362.5 | 2345.3 | 881.5 | 233.6 | 2635.9 |
| 1/2 | 84.0 | 98.8 | 1030.2 | 225.0 | 63.2 | 947.6 |
| 1/4 | 21.8 | 25.3 | 349.1 | 57.0 | 17.6 | 284.3 |
| 1/8 | 5.4 | 6.3 | 96.5 | 14.7 | 5.7 | 77.6 |

Table 6: Comparison of different weighting schemes for the Born Ion

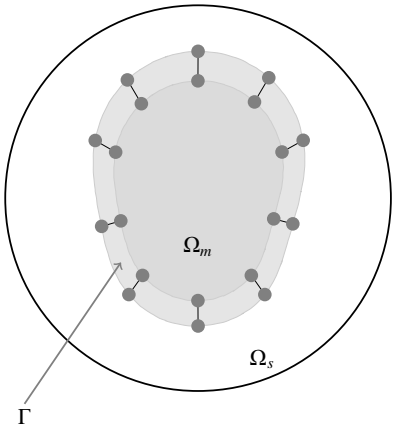


Figure 5: Schematic of the interfacial degrees-of-freedom for the dual domain formulation

$1/\sqrt{\epsilon}$ weighting results in improved conditioning in the systems for all ranges of the ratios considered, as shown in Figure 6a. Moreover, we see from Figure 6b that the growth in conditioning is only linear, although in the limit the conditioning grows with a factor of two as predicted by the theory. Moreover, while a weighting of 1.0 results in low growth in the condition number, the convergence for this weighting is not competitive, as shown in Table 6. From now on in this article, we use the weighting $\alpha = 1/\sqrt{\epsilon}$, unless otherwise specified.

## 7. Convergence of the Least-Squares Method

In this section, we explore the convergence properties of the weighted LSFEM discretization developed in the previous section. We also discuss several quantitative implications such as the ability of the least-squares approximation to attain physical quantities—e.g. solvation energy—that are consistent with that of Galerkin. To this end, we include several results using a standard Galerkin method as a baseline to highlight the potential of the least-squares approach. The Galerkin approximation for the regularized PBE is defined by the weak problem: find $u$ so that

$$\int_\Omega \epsilon \nabla u \cdot \nabla v + \bar{\kappa}^2 uv \, d\mathbf{x} = \int_\Omega -(\epsilon - \epsilon_m)\nabla u_c \cdot \nabla v - \bar{\kappa}^2 \nabla u_c v \, d\mathbf{x}, \qquad \forall\, v.$$

Notice that the flux variable is not explicitly expressed in the weak form— i.e. only the scalar potential $u$ is represented. As such, we examine the $L^2$ convergence of the error in the scalar potential and its gradient for both the Galerkin and the least-squares finite element approximations.

Table 8 shows that both approximations achieve optimal $O(h^2)$ convergence for the scalar potential of the Born ion (recall the analytic solution is available in this case). The difference is in representing the flux. The Galerkin approximation

| | Born Ion | Methanol |
|---|---|---|
| $\alpha = 1/\epsilon$ | 8.07E+09 | 8.66E+09 |
| $\alpha = 1/\sqrt{\epsilon}$ | 1.05E+08 | 1.12E+08 |

Table 7: Conditioning of the linear systems for different weightings

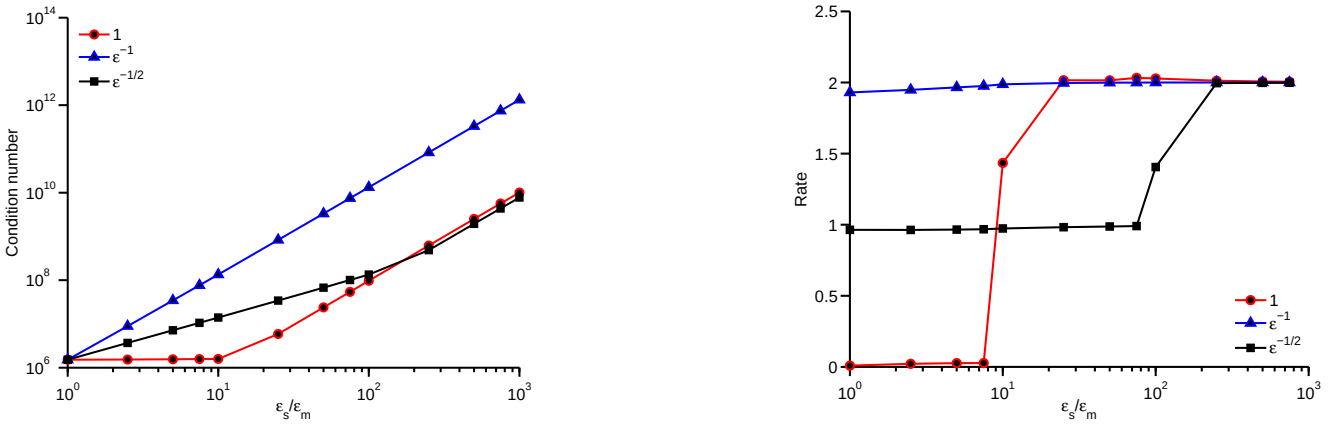


(a) Condition numbers

(b) Rate of growth

Figure 6: Dependence of the conditioning on the ratio $\epsilon_s/\epsilon_m$ for different weightings

is only $O(h)$, while the least-squares approach yields $O(h^2)$ convergence. Here, the gradient is reconstructed for the Galerkin approximation using a simple piecewise constant representation, however for both methods high-order approximations to the gradient are possible [24].

| | $u$ | | | | $\nabla u$ | | | |
|---|---|---|---|---|---|---|---|---|
| | Galerkin | | LS | | Galerkin | | LS | |
| $h/h_0$ | Value | Rate | Value | Rate | Value | Rate | Value | Rate |
| 1 | 346.7 | | 362.5 | | 358.5 | | 51.1 | |
| 1/2 | 94.3 | 1.88 | 98.8 | 1.87 | 186.8 | 0.94 | 14.0 | 1.86 |
| 1/4 | 24.2 | 1.96 | 25.3 | 1.96 | 94.0 | 0.99 | 3.5 | 1.96 |
| 1/8 | 6.0 | 2.01 | 6.3 | 2.00 | 46.8 | 1.01 | 0.8 | 2.00 |

Table 8: $L^2$ convergence of $u$ and $\nabla u$ for the Born Ion

*Solvation Free Energy Calculations*

The electrostatic free energy of solvation measures the difference between electrostatic energy in solution and in vacuum [32]. For a set of discrete charges $Q_i$ and regularized potential $u$, the electrostatic free energy [12, 33] is defined by

$$\triangle G_{sol} = \frac{1}{2}\frac{k_B T}{e_c}\sum_{i=1}^{n_c} Q_i u(\mathbf{x}_i). \tag{25}$$

Figure 7 shows the solvation free energy results for the three schemes: Galerkin with uniform refinement and labeled "Galerkin", LSFEM with uniform refinement and labeled "LS" and LSFEM with adaptive refinement and labeled "Adaptive LS". The adaptive refinement algorithm is also used in [12], and is based on the least-squares functional estimator. In each plot, the solvation free energy is shown as a function of $N^{1/3}$, where $N$ is the number of nodes in the mesh. The results indicate that both Galerkin and LSFEM have similar rates of convergence. Moreover, this shows that the least-squares approach benefits from the use of adaptive refinement; this has also been demonstrated for the Galerkin method applied to the PBE [34].

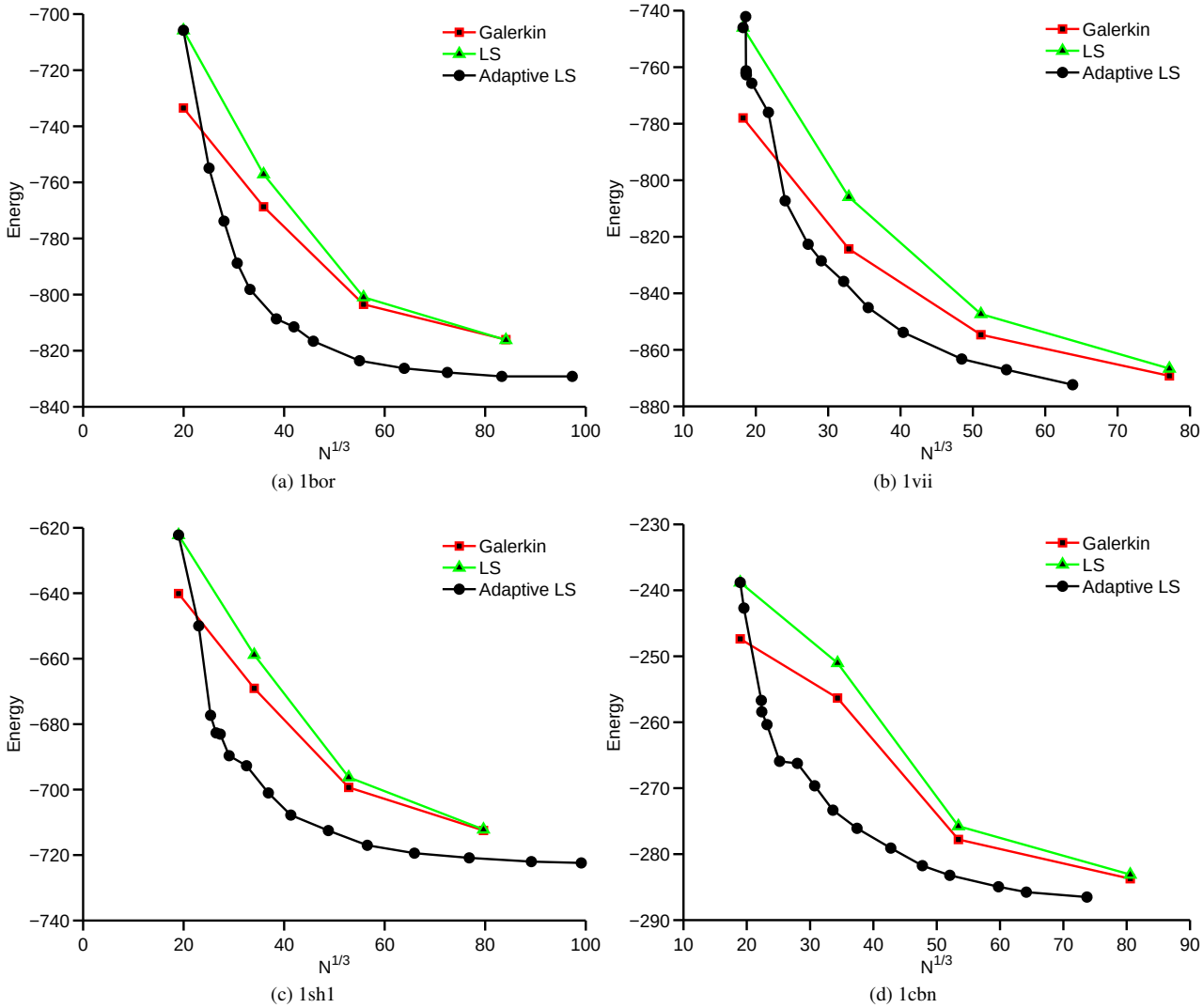


Figure 7: Comparison of the "Galerkin", "LS" and "Adaptive LS" methods for computing solvation free energy.

**Remark 2.** *It is known that if the interfacial boundary is not differentiable, then the solution exhibits singularities at corners [16]. The solution of the Poisson-Boltzmann equation is known to be sensitive to the description of the solvent–molecular interface (or molecular surface) [6]. This interface is used to model the inability of solvent to penetrate the molecule, and is typically defined as a unions of spheres, splines, or a level set [6]. During mesh refinement, there are two methods for adding new points to the mesh. In one case, they are simply placed at midpoints of edges in the parent mesh. The concern here is that we are limited by the initial definition of the mesh. The other option is that the new points that are introduced through refinement are pushed to the true interface, thereby ensuring a smoother surface in the limit. A disadvantage of this approach is that the meshes are not nested and that more management is needed during refinement. Moreover, in some situations simplices at the surface may exhibit flattening. To overcome flattening of elements the mesh may require additional smoothing. We find that with the least-squares finite element methods, that the convergence of the least-squares norm is maintained in either case of refinement, highlighting the robustness of the approach.*

## 8. Conclusions

In this article we examined the numerical properties of a least-squares finite element method (LSFEM) for the linear Poisson-Boltzmann equation. The least-squares functional we considered is $H(\mathrm{div}) \times H^1$ equivalent, which motivated our investigation of $H(\mathrm{div})$ conforming Raviart–Thomas elements for the flux variable. The $RT_0$ element yields optimal convergence. We then investigated different weightings of the LSFEM functional and concluded that weighting the flux equation by $1/\sqrt{\epsilon}$ yielded improved approximation properties over the natural splitting.

Least-squares yields an accurate approximation to scalar variables and physical quantities such as solvation free energy. Moreover, we observe improved control of the gradient of the solution in the LSFEM, and hence advocate this approach when evaluation of solution derivatives is desired. Through our discussion we concluded that LSFEMs are both accurate and computationally tractable.

## References


[1] G. Gouy, Sur la constitution de la charge électrique a la surface d'un électrolyte, J. Phys. Theor. Appl. 9 (1910) 457–468.
[2] D. L. Chapman, A contribution to the theory of electrocapillarity, Philosophical Magazine 25 (148) (1913) 475–481.
[3] M. E. Davis, J. A. McCammon, Electrostatics in biomolecular structure and dynamics, Chem. Rev. 90 (3) (1990) 509–521.
[4] P. Koehl, Electrostatics calculations: Latest methodological advances, Curr. Opin. Struc. Biol. 16 (2) (2006) 142–151.
[5] C. L. Vizcarra, S. L. Mayo, Electrostatics in computational protein design, Curr. Opin. Chem. Biol. 9 (6) (2005) 622–626.
[6] N. A. Baker, D. Bashford, D. A. Case, Implicit solvent electrostatics in biomolecular simulation, in: B. Leimkuhler, C. Chipot, R. Elber, A. Laaksonen, A. Mark, T. Schlick, C. Schutte, R. Skeel (Eds.), New Algorithms for Macromolecular Simulation, Vol. 49 of Lecture Notes in Computational Science and Engineering, Springer-Verlag, 2006, pp. 263–295.
[7] C. M. Cortis, R. A. Friesner, Numerical solution of the Poisson-Boltzmann equation using tetrahedral finite-element meshes, J. Comput. Chem. 18 (1997) 1591–1608.
[8] W. Chen, Y. Shen, Q. Xia, A mortar finite element approximation for the linear Poisson-Boltzmann equation, Appl. Math. Comput. 164 (1) (2005) 11–23.
[9] M. J. Holst, N. A. Baker, F. Wang, Adaptive multilevel finite element solution of the Poisson-Boltzmann equation I: Algorithms and examples, J. Comput. Chem. 21 (2000) 1319–1342.
[10] N. A. Baker, M. J. Holst, F. Wang, Adaptive multilevel finite element solution of the Poisson-Boltzmann equation II: Refinement at solvent accessible surfaces in biomolecular systems, J. Comput. Chem. 21 (2000) 1343–1352.
[11] A. I. Shestakov, J. L. Milovich, A. Noy, Solution of the nonlinear Poisson-Boltzmann equation using pseudo-transient continuation and the finite element method, J. Colloid Interf. Sci. 247 (1) (2002) 62–79.
[12] S. D. Bond, J. H. Chaudhry, E. C. Cyr, L. N. Olson, A first-order system least-squares finite element method for the Poisson-Boltzmann equation, J. Comput. Chem. 31 (8) (2010) 1625–1635.
[13] P. B. Bochev, M. D. Gunzburger, Finite element methods of least-squares type, SIAM Rev. 40 (4) (1998) 789–837.
[14] Z. Cai, R. Lazarov, T. A. Manteuffel, S. F. McCormick, First-order system least squares for second-order partial differential equations. I, SIAM J. Numer. Anal. 31 (6) (1994) 1785–1799.
[15] Z. Cai, T. A. Manteuffel, S. F. McCormick, First-order system least squares for second-order partial differential equations. II, SIAM J. Numer. Anal. 34 (2) (1997) 425–454.
[16] T. A. Manteuffel, S. F. McCormick, G. Starke, First-order system least-squares for second order elliptic problems with discontinuous coefficients, in: N. D. Melson, T. A. Manteuffel, S. F. McCormick, C. C. Douglas (Eds.), Seventh Copper Mountain Conference on Multigrid Methods, Vol. CP 3339, NASA, Hampton, VA, 1996, pp. 535–550.
[17] M. Berndt, T. A. Manteuffel, S. F. McCormick, G. Starke, Analysis of first-order system least squares (FOSLS) for elliptic problems with discontinuous coefficients. I, SIAM J. Numer. Anal. 43 (1) (2005) 386–408.
[18] M. Berndt, T. A. Manteuffel, S. F. McCormick, Analysis of first-order system least squares (FOSLS) for elliptic problems with discontinuous coefficients. II, SIAM J. Numer. Anal. 43 (1) (2005) 409–436.
[19] L. Chen, M. J. Holst, J. Xu, The finite element approximation of the nonlinear Poisson-Boltzmann equation, SIAM J. Numer. Anal. 45 (6) (2007) 2298–2320.
[20] F. Brezzi, M. Fortin, Mixed and hybrid finite element methods, Vol. 15 of Springer Series in Computational Mathematics, Springer-Verlag, New York, 1991.
[21] P. A. Raviart, J. M. Thomas, A mixed finite element method for second order elliptic problems, in: A. Dold, B. Eckmann (Eds.), Mathematical aspects of finite element methods, Vol. 606 of Springer Lecture Notes in Mathematics, Springer-Verlag, 1977, pp. 292–315.
[22] J.-C. Nédélec, Mixed finite elements in $R^3$, Numerische Mathematik 35 (3) (1980) 315–341.
[23] Z. Yu, M. J. Holst, Y. Cheng, J. A. McCammon, Feature-preserving adaptive mesh generation for molecular shape modeling and simulation, J. Mol. Graph. Model. 26 (8) (2008) 1370–1380.
[24] P. B. Bochev, M. D. Gunzburger, Least-Squares Finite Element Methods, Vol. 166 of Applied Mathematical Sciences, Springer, 2009.
[25] J. G. Kirkwood, Theory of solutions of molecules containing widely separated charges with special application to zwitterions, J. Chem. Phys. 2 (7) (1934) 351–361.
[26] M. J. Holst, Multilevel methods for the Poisson-Boltzmann equation, Phd, University of Illinois at Urbana-Champaign (1994).
[27] N. A. Baker, D. Sept, S. Joseph, M. J. Holst, J. A. McCammon, Electrostatics of nanosystems: Application to microtubules and the ribosome, Proc. Natl. Acad. Sci. USA 98 (2001) 10037–10041.
[28] H. M. Berman, J. Westbrook, Z. Feng, G. Gilliland, T. N. Bhat, H. Weissig, I. N. Shindyalov, P. E. Bourne, The protein data bank, Nucleic Acids Res. 28 (2000) 235–242, http://www.pdb.org.
[29] D. N. Arnold, R. S. Falk, R. Winther, Multigrid in $H$(div) and $H$(curl), Numer. Math. 85 (2) (2000) 197–217.
[30] R. Hiptmair, Multigrid method for H(div) in three dimensions, Electronic Trans. Numer. Anal. 6 (1997) 133–152.
[31] Y. Cao, M. D. Gunzburger, Least-squares finite element approximations to solutions of interface problems, SIAM J. Numer. Anal. 35 (1) (1998) 393–405.
[32] M. Feig, A. Onufriev, M. S. Lee, W. Im, D. A. Case, C. L. Brooks III, Performance comparison of generalized Born and Poisson methods in the calculation of electrostatic solvation energies for protein structures, J. Comput. Chem. 25 (2) (2004) 265–284.
[33] W. Geng, S. Yu, G. Wei, Treatment of charge singularities in implicit solvent models, J. Chem. Phys. 127 (11) (2007) 114106.
[34] B. Aksoylu, S. D. Bond, E. C. Cyr, M. J. Holst, Goal-oriented adaptivity and multilevel preconditioning for the Poisson-Boltzmann equation, J. Sci. Comput. (2011) to appear.